High-Throughput Computational Assessment of Previously Synthesized Semiconductors for Photovoltaic and Photoelectrochemical Devices

Kuhar, Korina; Pandey, Mohnish; Thygesen, Kristian Sommer; Jacobsen, Karsten Wedel

Published in:
ACS Energy Letters

Link to article, DOI:
10.1021/acsenergylett.7b01312

Publication date:
2018

Document Version
Peer reviewed version

High-Throughput Computational Assessment of Previously Synthesized Semiconductors for Photovoltaic and Photoelectrochemical Devices.

Korina Kuhar,[†] Mohnish Pandey,[*,†] Kristian S. Thygesen,[†,‡] and Karsten W. Jacobsen[*,†]

†*Computational Atomic-scale Materials Design (CAMD), Department of Physics, Technical University of Denmark, DK - 2800 Kongens Lyngby, Denmark*

‡*Center for Nanostructured Graphene (CNG), Department of Physics, Technical University of Denmark, DK - 2800 Kongens Lyngby, Denmark*

E-mail: mohpa@fysik.dtu.dk; kwj@fysik.dtu.dk

Abstract

Using computational screening we identify materials with potential use as light absorbers in photovoltaic or photoelectrochemical devices. The screening focuses on compounds of up to three different chemical elements, which are abundant and non-toxic. A prescreening is carried out based on information from the ICSD and OQMD databases. The light absorption, carrier mobility, defect tolerance, and stability of the materials are assessed by a set of simple computational descriptors. The identified 74 materials include a variety of pnictogenides, chalcogenides, and halides. Several recently investigated light absorbers such as $CsSnI_3$, $CsSnBr_3$, and $BaZrS_3$ appear on the list.

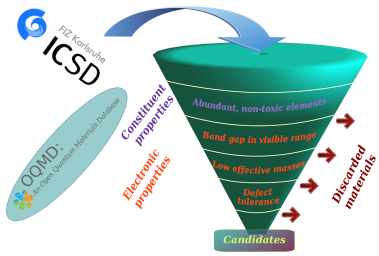

The increasing demand for energy to supply the growing human population has led to large-scale consumption of fossil fuels. As a result, the emission of greenhouse gases into the atmosphere is having detrimental effects on the environment. Therefore, it is an urgent requirement to explore fossil-free energy resources. One of the most promising such resources is the solar energy. Although, solar energy may not be able to fully substitute the fossil fuels in the near future, it has the potential to alleviate the environmental problems if used at a global scale. There are numerous ways to harvest the solar energy such as photovoltaics (PV), photoelectrochemical (PEC) generation of hydrogen or other chemicals, and thermal fuels.[1–5] These technologies are still not fully developed and significant efforts are required for their large-scale deployment.

Solid-state PV and PEC processes rely on materials which absorb the solar photons, generate electrons and holes, and conduct them to surfaces to participate in chemical processes or deliver electric current. For a material to work in a reasonable way, these processes

must all be carried out efficiently. The PV technology relies predominantly on silicon as an absorber[6–8] in addition to a few other semiconductors such as GaAs, CdTe, InP, GaInP, CZTS(Se) and CIGS.[6,7,9–12] The deployment of PV technology is rapidly growing, while the PEC technology has not been realized yet mainly due to the lack of materials which can efficiently harvest visible light and use the generated electron-hole pair to for example split water. However, numerous materials have been explored for PEC, to name a few; TiO_2, CdS, Bi_2S_3, Sb_2S_3,WO_3, ZnO, Cu_2ZnSnS_4 and Fe_2O_3.[13–15] Despite numerous attempts, an analog of silicon for PEC has not been found yet. In order to address the challenges hampering the PEC technology alternative strategies are continuously being explored. One such strategy is to integrate existing silicon PV devices into PEC units. In these "tandem" devices two semiconductors with different band gaps (one of them being for example silicon) are used as photoanode and photocathode, each conducting one half of the water-splitting reaction.[16–20]

Despite the considerable research efforts the number of semiconductors, which have been explored for PV or PEC, is still small compared to the number of semiconductors, which have been synthesized. Therefore, a systematic investigation of the properties of already known semiconductors may reveal new interesting materials for PV or PEC application. However, performing experimental investigation of all relevant properties for thousands of materials is a daunting task, and this is where computational screening approaches can provide useful guidelines.[21,22]

In the past few years, publicly available databases with calculated properties of hundreds of thousands of materials have been established.[23–28] However, some of the properties like band gaps or charge carrier effective masses, which are relevant to PV and PEC applications, are either not reported or the reported values are not very accurate due to limitations of the methods used. In the present work, we use the data reported in the Open Quantum Materials Database (OQMD)[23,24] and then take a step further to calculate relevant electronic properties of already synthesized materials. The criteria we use to screen the materials are based on the toxicity and abundance of constituent elements, thermodynamic stability, band

gap in the visible spectrum, high charge carrier mobility, and small tendency of the materials to exhibit defect-mediated mid-gap states in the band gap. Based on the criteria, we suggest new candidates which can potentially act as PV and PEC light absorbers.

The electronic structure calculations are performed using Density Functional Theory (DFT) in the Projector Augmented Wave (PAW) formalism[29] as implemented in the electronic structure code GPAW[30,31] with the ASE interface.[32,33] The wave functions, electron density and the effective potential are expanded on a real space grid with a grid spacing of 0.18 Å. The sampling of the Brillouin zone is performed using the Monkhorst-Pack scheme.[34] The k-point density is chosen to be 5 points $Å^{-1}$, and finer k-point meshes are adopted for the calculation of band structures and effective masses. The band gaps and band structures are calculated using the more accurate semi-local Gritsenko, van Leeuwen, van Lenthe and Baerends potential (GLLB) improved for solids (-SC), which includes an explicit estimation of the derivative discontinuity.[35,36] The GLLB-SC functional with similar computational cost as the other semi-local functionals predicts band gaps, which are quite close to the predictions of more computationally demanding many-body-perturbation-theory calculations and hybrid functionals.[37] Spin-orbit coupling was included in the calculations for materials containing elements with atomic number (Z) higher than 56. Investigation of defect properties was done with the PBE exchange correlation functional.[38] It should be noted that due to self-interaction errors in the PBE functional the quantitative description of the defects cannot be expected to be accurate. Therefore, the analysis should only be considered qualitative.

The Inorganic Crystal Structure Database[39] is a library of over 180000 inorganic compounds, where most of the compounds have been experimentally synthesized. The OQMD database is a computational materials database, which contains information about a large fraction of the crystal structures present in the ICSD. In the following we shall take as the starting point the materials in OQMD which originates from the ICSD. This limitation to the materials that appear in both ICSD and OQMD has several advantages: 1) As mentioned by-far most of the materials in ICSD have been synthesized, so this means that they can be

considered stable or at least meta-stable. We do therefore not investigate material stability any further in the screening process, which saves considerable computer time. However, in the final stage of the screening we return to the stability issue, because some of the compounds have been synthesized only under extreme conditions. 2) In ICSD many materials appear several times as duplicates, but these have been removed in OQMD. 3) The materials in OQMD have already been structurally optimized within the DFT framework using the PBE functional so that atomic forces and stresses vanish. This is convenient for further computational investigation. 4) Several properties like the band gaps of the compounds have already been calculated at the PBE-level, which we shall also exploit.

The initial download from the OQMD contained 28,566 compounds to be considered [1]. These compounds are uniquely identified by their ICSD numbers, which are also provided in the OQMD database. We shall here limit ourselves to compounds of up to three elements of which there are 22,807.

We now begin a screening funnel, where we gradually remove compounds, which do not seem promising according to a list of criteria. The first step of the funnel is to restrict ourselves to compounds, which are made of only abundant and non-toxic elements for which an open market exists. We use the analysis by Gaultois *et al.*,[40] which is based on the crustal abundance of the elements and the so-called Herfindahl-Hirschman index (HHI) as a measure of the concentration or monopoly-character of the resources and the market. A priority list of elements based on these criteria are shown in Figure 1 and the resulting elements are also indicated in blue in the table of elements in Figure 2.

The abundance and toxicity criteria for the elements lead to a reduction in the number of compounds from 22,807 to 7,241. In the next step of the screening funnel we benefit from the fact that the Kohn-Sham band gaps have already been calculated and reported in the OQMD database using the PBE functional. It is well known that band gaps calculated with the PBE are severely underestimated, so we therefore use these band gaps only in a semi-quantitative

[1] We acquired the dataset from the OQMD database around October 2014. At that time the ICSD-entries in the OQMD included systems with up to 35 atoms in the primitive unit cell.

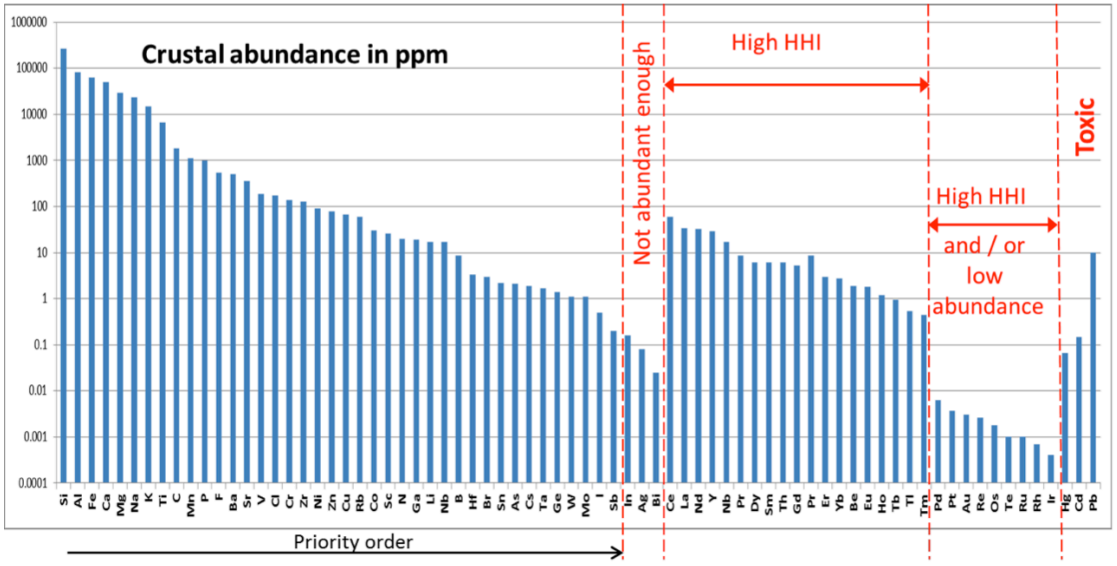

Figure 1: The list of elements to be considered in the screening study based on crustal abundance and the Herfindahl-Hirschman index (HHI).[40]

way. We first discard all compounds without a PBE band gap, i.e the compounds which according to PBE are metallic. It should be noted that some compounds, for example several oxides, are in reality semiconductors or insulators despite a vanishing PBE band gap because of strong correlation effects. Such compounds are therefore not included in the screening. Additionally, we exploit the underestimation of the PBE band gaps to discard materials which have PBE band gaps higher than 2.0 eV. The optimal band gap for single junction PV devices is $\sim$1 eV, which we shall refer to as a small band gap (SBG), whereas the tandem devices require for their large band gap component (LBG) a band gap of $\sim$2.0 eV.[18] This leads us to focus on materials with band gaps between 0.5 eV and 2.5 eV. It is quite unlikely that a material with a PBE band gap of more than 2 eV does in fact have an experimental band gap of less than 2.5 eV, so these materials are discarded. The number of candidate materials is reduced to 1630 by this step. The procedure is schematically shown in Figure 2.

We now move on to consider a proper evaluation of the band gaps of the materials. As mentioned above, the PBE functional severely underestimates the band gaps and cannot therefore be used for realistic prediction. The underestimation is due mainly to the neglect of the so-called derivative discontinuity, which corrects the Kohn-Sham gap to obtain the fundamental gap. The GLLB-SC functional improves on this by including an explicit calculation of the derivative discontinuity.[35,36] The GLLB-SC functional gives a reasonable estimate of the band gaps within $\approx 0.3 - 0.5$ eV as demonstrated in previous work with comparisons to experiment and to G_0W_0 and HSE06 calculated band gaps.[37]

The GLLB-SC functional has convergence issues and maybe also more fundamental problems for magnetic systems, and we therefore concentrate on the spin-paired semiconductors. This reduces the number of candidate materials from 1,630 to 929. This is a significant reduction and it would be interesting in future work to investigate also the 701 spin-polarized compounds. In Figure 3(a) we show the GLLB-SC calculated values of the band gaps versus the PBE band gaps. The figure clearly shows that the GLLB-SC band gaps are larger than

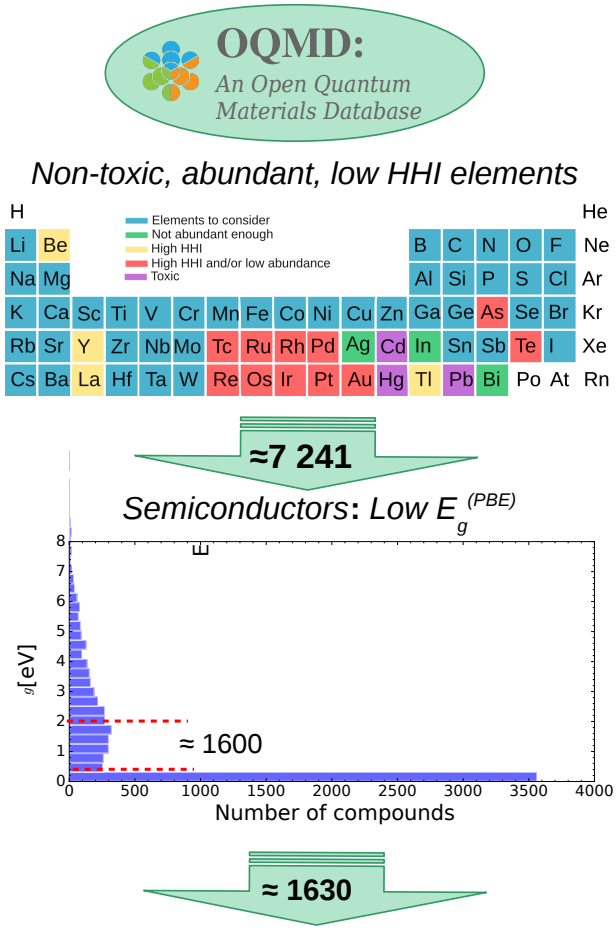

Figure 2: Flow of data selection process: Entries are extracted from the OQMD database (22,807 that originate from the ICSD with up to three elements), only entries containing non-toxic, abundant and low HHI elements are to be considered further. Furthermore, the number of candidates is additionally decreased by selecting only semiconducting materials with 0 eV$< \mathrm{E}_g^{PBE} \leq 2$ eV, containing up to three elements resulting in 1,630 candidates.

the PBE calculated values in most cases and that it is unlikely that materials with a PBE band gap above 2 eV could have a GLLB-SC band gap in the relevant range. Based on the GLLB-SC predicted band gaps we identify 323 LBG and 195 SBG materials for further consideration.

Efficient transport of the generated charge carriers after light absorption is required for low losses in a PV/PEC material. The losses mainly arise due to recombination of charge carriers, which can potentially be prevented if the charges separate and move apart fast enough after their generation. Therefore, high mobilities are a prerequisite for efficient charge transport and should dampen the losses due to recombination. Several mechanisms can limit the carrier mobilities including scattering by phonons, electrons, or defects, but direct calculation of the scattering times associated with these different mechanisms is difficult and computationally demanding in particular for large systems. However, independent of the scattering mechanism and the scattering life time, the mobilities are inversely proportional to the effective charge carrier masses, and we shall therefore use the effective electron and hole masses as descriptors for the mobilities. The situation is more complicated if polaron hopping is the main transport mechanism. However, the formation of polarons involves electron localization, and a low effective mass is indication of highly delocalized states which make the localization less likely.

The carrier effective masses are obtained by fitting a parabola to the top of the valence band and bottom of the conduction band of the band structure. The band structures are calculated along the high-symmetry band path as suggested by Setyawan and Curtarolo.[41] At high-symmetry points where the band path changes directions, parabolic fits are made on both sides of the symmetry point. We choose an upper limit for both the effective electron and hole masses to be one standard electron mass. Figure 3 (b) shows a combined histogram of all the materials with band gaps in the relevant range (green) and the ones with low effective masses (blue). This step decreases the number of materials from 518 (with appropriate band gap) to 222 materials, which additionally satisfy the criterion for the

effective mass.

Figures 4 and 5 show the band gaps of the binary and ternary PV and PEC materials satisfying the criteria introduced so far. The selection process so far identifies several materials which are well-known light absorbers such as ZnS, ZnS_2, FeS_2, $CsSnI_3$ and, $ZnSiP_2$. This, to some extent, validates our approach. At the end of the screening process, we shall consider other well-known light absorbers, which do not appear as candidates and discuss the reasons for this.

The final step in the screening funnel takes defect properties into account. Defects can be detrimental to the performance of semiconductors as PV/PEC materials. For example, the defects present in FeS_2 act as recombination centers, which severely deteriorates its performance.[42] Generally, presence of different defects like vacancies, substitutional defects, and impurities may give rise to new electronic states in the band gap, which reduces the photo-absorption or they act as recombination centers.[43] The materials exhibiting this kind of behavior are commonly termed "defect-sensitive", whereas semiconductors which only show nominal change in their electronic structure upon introducing defects are termed "defect-tolerant".[43–46]

In the following we aim to identify the defect-tolerant materials by explicit calculation of the electronic structure in the presence of defects. Ideally, defect calculations require large supercells with different charge state along with careful incorporation of electrostatic corrections to the electronic structure and energies.[47–51] However, such accurate defect calculations are computationally too demanding for a screening study like the present one, and, furthermore, we are not aiming to study defect properties in detail, but only to determine whether a given material is defect tolerant or not. We have previously proposed a simple descriptor for defect tolerance, which uses the orbital character of the conduction and valence bands of the pristine semiconductor to infer whether or not the band gap has bonding/anti-bonding character.[44] The method was successfully applied to a class of metal-dichalcogenides, but we have found it to be less applicable to the heterogeneous class of materials investigated here.

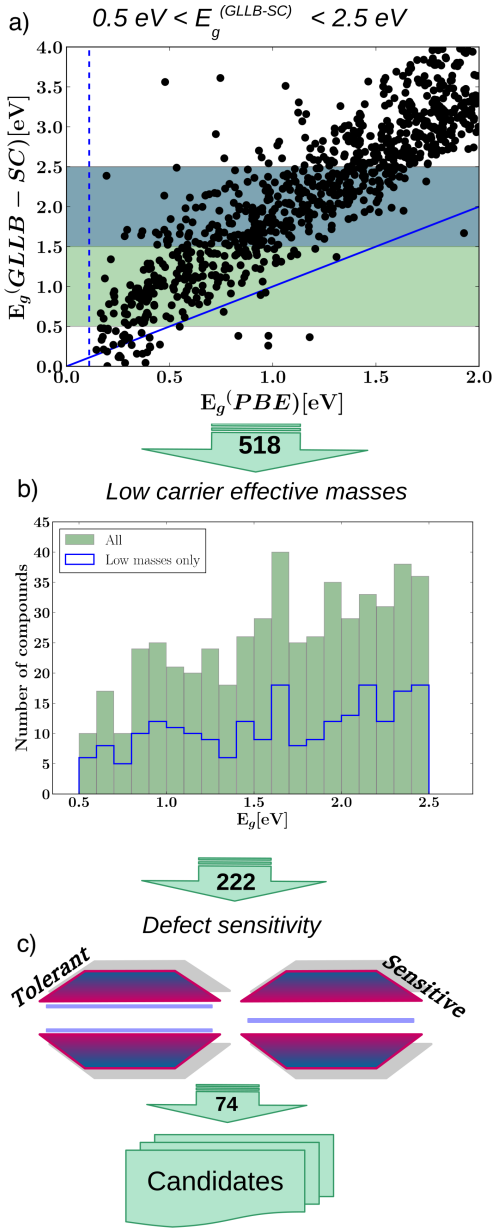

Figure 3: Schematic view of the step-wise inclusion of new descriptors. a) Selecting materials with the GLLB-SC calculated band gaps in the range between 0.5 and 2.5 eV. The plot shows the GLLB-SC band gaps versus the PBE band gaps. The blue and green striped areas show the HBG and LBG regions, respectively. b) Selection of the compounds with the carrier effective masses less than one standard electron mass. The histogram of the band gaps of the materials before and after applying the criterion for the effective mass. c) Selection of the defect tolerant materials. Defect tolerance refers to the situation when no mid gap states in the band structure arise as a result of presence of point defects in the crystal. Numbers written on the arrows represent the number of candidates in each step.

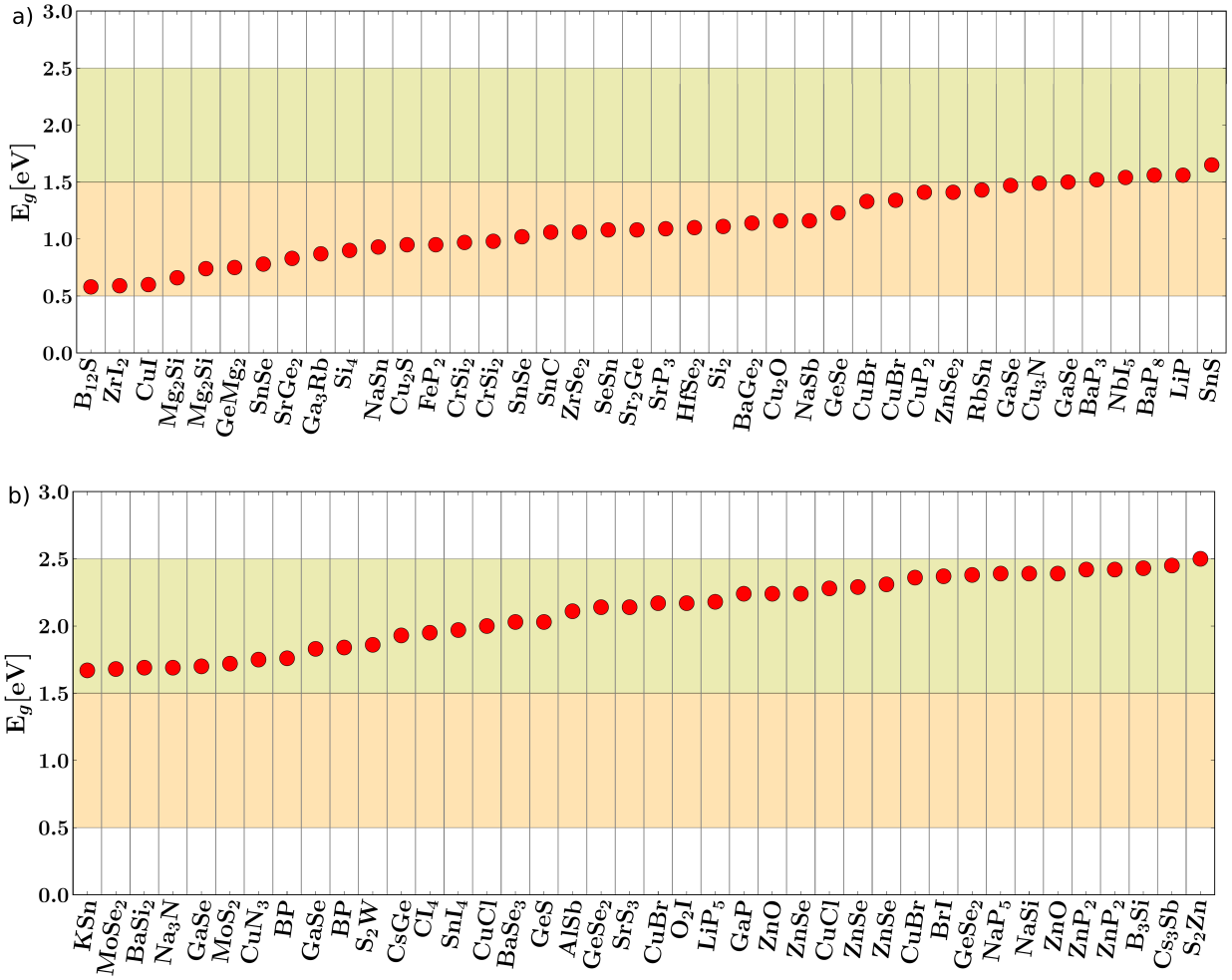

Figure 4: Calculated band gaps of binary systems satisfying the screening criteria for abundance, non-toxicity, light absorption, and mobility. Due to a long list of materials the figure is divided into a) and b). The materials are arranged according to increasing order of the band gap, with the smallest ones in a) and the larger ones in b). Orange and green areas represent LBG and HBG regions, respectively. A table with numerical values and ICSD codes can be found in the supporting information (SI).

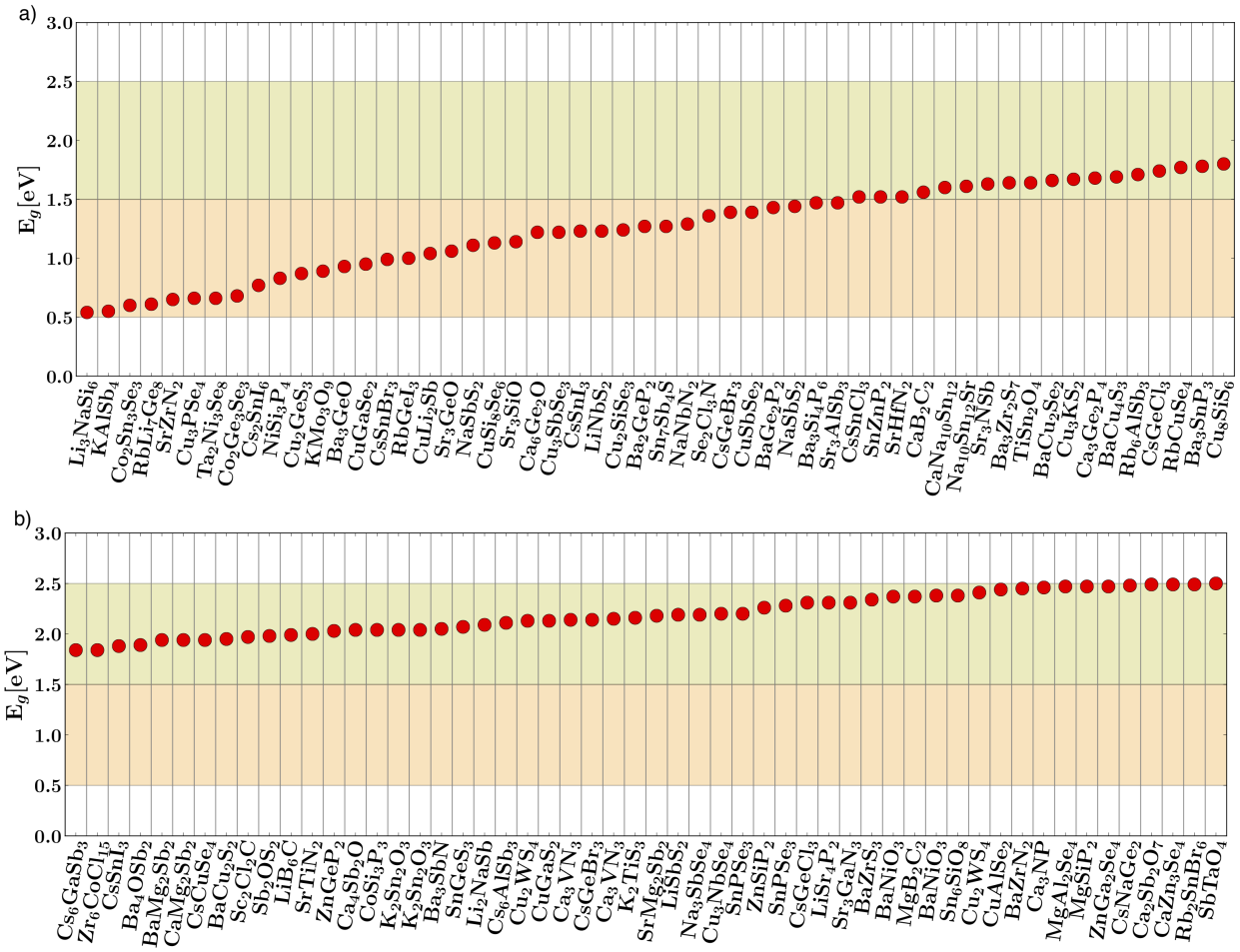

Figure 5: Calculated band gaps of ternary systems satisfying the screening criteria for abundance, non-toxicity, light absorption, and mobility. Due to the long list of materials the figure is divided into a) and b). The materials are arranged according to increasing order of the band gap, with the smallest ones in a) and the larger ones in b). Orange and regions represent LBG and HBG regions, respectively. Table with numerical values and ICSD codes can be found in the SI.

We limit ourselves to study vacancy defects in their neutral states by creating one defect in repeated 2×2×2 (or 3×3 ×3 if the pristine unit cell is smaller than 5 atoms) supercells. Vacancies for all the constituent elements are investigated. The density of states (DOS) is then calculated in the defect supercell without relaxing the atomic structure after defects are introduced. The calculations are performed using the LCAO-mode of GPAW with a dzp basis set.[52] If the resulting DOS resembles the DOS of the pristine structure i.e. there are no mid-gap states in the band gap (or only shallow states near the band edges), we consider the material as defect-tolerant. This approach does not rule out that other kinds of defects can harm the photoelectric performance, but at least it removes from the screening funnel the ones where the vacancies lead to mid-gap states.

Table 1: Final list of suggested PV and PEC candidates including the calculated band gaps and effective masses, and, if available, experimental band gaps. The energies of the compounds with respect to the convex hulls ΔH_{hull} (eV/atom) are also reported. A large positive value of ΔH_{hull} implies that the compound may not be stable under normal conditions. Compounds with $\Delta H_{hull} > 0.05$ eV are shown in parenthesis. The corresponding ICSD numbers of all the compounds are provided in the SI. For the compounds labelled by asterisks the investigations of defect sensitivities are inconclusive, because the PBE/LCAO gaps are too narrow to allow for a clear distinction between mid-gap and shallow states. The band gaps are reported in eV and the effective masses in the units of electron's rest mass m_e.

Formula	$E_g^{GLLB-SC}$ (eV)	$E_{g(direct)}^{GLLB-SC}$ (eV)	m^*_h (m_e)	m^*_e (m_e)	$E_g^{exp.}$ (eV)	ΔH_{hull} (eV/atom)
Al_2MgSe_4*	2.47	2.47	0.38	0.21	-	0.01
$(B_{12}S)$*	0.58	0.75	0.40	0.29	-	0.41
Ba_3P_4	1.07	1.07	0.95	0.97	1.6 [53]	0.00
Ba_3SbN	2.05	2.05	0.18	0.25	-	0.00
Ba_5Sb_4	0.94	1.27	0.66	0.36	-	0.00
Ba_4SnP_4	1.78	1.79	0.32	0.47	-	0.01
BaCaSn	0.88	0.88	0.34	0.73	-	0.00
BaLiP	1.98	1.98	0.16	0.16	-	0.00
$BaZrN_2$	2.45	2.45	0.38	0.28	-	0.00
$BaZrS_3$	2.34	2.34	0.35	0.43	1.8 [54,55]	0.00
Ca_3NP	2.46	2.46	0.21	0.29	-	0.00
CaLiSb	1.36	1.36	0.13	0.40	-	0.00
Cs_2SnI_6*	0.77	0.77	0.84	0.26	1.3 [56]	0.00
Cs_3Sb	2.45	2.75	0.76	0.23	1.6(300K) [57]	0.00
Cs_6AlSb_3	2.11	2.21	0.91	0.28	-	0.00
Cs_6GaSb_3	1.84	1.94	0.99	0.29	-	0.00
$CsCuSe_4$	1.94	2.01	0.48	0.26	-	0.00
CsGe Cl_3	2.31	2.31	0.27	0.29	-	0.00
$CsNaGe_2$	2.48	2.51	0.35	0.51	-	0.00

Table 1 – continued from previous page

Formula	$E_g^{GLLB-SC}$ (eV)	$E_{g(direct)}^{GLLB-SC}$ (eV)	m^*_h (m_e)	m^*_e (m_e)	$E_g^{exp.}$ (eV)	ΔH_{hull} (eV/atom)
$CsSnBr_3$	0.99	0.99	0.09	0.08	1.26 [58]	0.00
$CsSnI_3$ (B)	1.23	1.23	0.10	0.06	1.3 (GW 1.3) [59,60]	0.00
$CsSnI_3$	1.88	1.88	0.12	0.09	-	0.00
(CuI)	0.6	1.39	0.71	0.36	-	0.07
(Cu_3N)	1.49	2.00	0.24	0.21	1.5 [61]	0.24
Cu_2S	0.95	0.95	0.26	0.15	1.2 [57]	0.01
Cu_3SbSe_3	1.22	1.27	0.52	0.44	1.68 [62]	0.03
Cu_8SiSe_6	1.13	1.15	0.46	0.19	1.33 [63]	0.05
Cu_2GeS_3	0.87	0.87	0.26	0.16	-	0.00
Cu_2O	1.16	1.16	0.25	0.78	2.17 [57]	0.00
Cu_3KS_2	1.67	1.74	0.36	0.40	-	0.00
$CuAlSe_2$	2.44	2.44	0.22	0.16	-	0.00
$CuGaS_2$	2.13	2.13	0.23	0.19	2.53 [64]	0.00
$CuKSe^*$	1.44	1.44	0.10	0.13	-	0.00
$CuSbSe_2$	1.39	1.59	0.77	0.56	1.2 [65]	0.00
Ga_2Se_3	2.02	2.02	0.21	0.16	1.9 [57]	0.00
Hf_3N_4	2.39	2.39	0.27	0.37	1.8 [66]	0.00
K_2P_3	1.89	1.91	0.79	0.99	-	0.00
$K_2Sn_2O_3$	2.04	2.04	0.22	0.15	-	0.00
KMo_3O_9	0.89	0.96	0.97	0.64	-	0.00
$KZnSb^*$	0.88	1.01	0.06	0.09		0.01
Li_2NaSb	2.09	3.38	0.13	0.24	-	0.00
Li_3NaSi_6	0.54	0.6	0.31	0.41	-	0.00
LiP	1.56	1.84	0.42	0.58	-	0.00
$LiSrN^*$	1.64	2.19	0.92	0.28	-	0.00
LiSrP	2.29	2.59	0.38	0.65	-	0.00
LiZnN	1.52	1.52	0.13	0.16	1.9 [67,68]	0.00
Mg_2Si^*	0.66	0.66	0.19	0.57	-	0.00
$Mg_3Sb_2{}^*$	1.1	1.91	0.10	0.23	1.1 [69]	0.00
Mg_2Ge	0.75	1.67	0.08	0.22	0.74 [57]	0.00
NaBaP	2.22	2.22	0.21	0.25	-	0.00
$NaNbN_2{}^*$	1.29	1.94	0.23	0.52	-	0.00
NbI_5	1.54	1.59	0.85	0.37	-	0.00
O_2I	2.17	2.69	0.72	0.77	-	0.02
Rb_2SnBr_6	2.49	2.49	0.82	0.37	-	0.00
Rb_6AlSb_3	1.71	1.79	0.95	0.24	-	0.00
$RbGeI_3$	1.00	1.00	0.09	0.07	-	0.03
$RbLi_7Ge_8{}^*$	0.61	0.67	0.71	0.48	-	0.00
RbSn	1.43	1.43	0.62	0.28	-	0.00
$SnPSe_3$	2.2	2.33	0.72	0.68	-	0.00
Sr_2Ge	1.08	1.08	0.13	0.61	-	0.00
$Sr_3\ AlSb_3$	1.47	1.47	0.59	0.44	-	0.00
Sr_3GaN_3	2.31	2.37	0.63	0.27	-	0.00
Sr_3GeO	1.06	1.06	0.10	0.17	-	0.00
Sr_3SbN	1.63	1.63	0.19	0.18	1.15 [70]	0.00
Sr_3SiO	1.14	1.14	0.14	0.19	-	0.00
$SrGe_2$	0.83	1.01	0.52	0.48	-	0.00
SrS_3	2.14	2.14	0.94	0.71	-	0.00
$SrZrN_2$	0.65	1.31	0.26	0.32	-	0.00
(ZnS_2)	2.5	2.83	0.47	0.46	2.5 (GW 2.7) [71]	0.08
($ZnSe_2$)	1.41	1.65	0.20	0.57	1.56 (GW 1.7) [71]	0.15
Zr_3N_4	2.13	2.13	0.32	0.38	2.1-2.3 [72]	0.05
$ZrI_2{}^*$	0.59	0.71	0.91	0.37	0.1 [73]	0.00

Table 1 – continued from previous page

Formula	$E_g^{GLLB-SC}$ (eV)	$E_{g(direct)}^{GLLB-SC}$ (eV)	m^*_h (m_e)	m^*_e (m_e)	$E_g^{exp.}$ (eV)	ΔH_{hull} (eV/atom)
ZrNI*	0.92	0.92	0.29	0.37	-	0.00
$ZrSe_2$*	1.06	1.91	0.29	0.29	1.2,1.6 [74]	0.00

This completes the screening funnel and the resulting candidates are shown in Table 1. In the following we shall discuss these materials and some of their properties in more detail. However, before doing so, we shall return to the issue of material stability. By far, most of the materials in ICSD have been experimentally synthesized and can therefore be regarded as stable or at least meta-stable. However, some of the materials are synthesized under extreme conditions of pressure or temperature and are therefore not necessarily stable under normal conditions. These materials might therefore decompose into competing phases, which are more stable. This issue can be assessed by the convex hull construction from the formation energies. The convex hull value at a given chemical composition is obtained by minimizing the linear combination of energies of all possible phases constrained to the given composition. If the compound lies significantly above the hull it is an indication of a potential problem with the stability under normal conditions. This might be due to high pressure/temperature synthesis, but can also be caused by other problems with the ICSD entry.

The relative stabilities, ΔH_{hull}, of the compounds with respect to the convex hull are shown in Table 1. The data are obtained directly from the OQMD database. If ΔH_{hull} is zero for a particular compound, then the compound is most likely stable under normal conditions whereas a large positive value imply possible instability. The compounds with ΔH_{hull} above 50 meV are shown in parenthesis. For example, CuI is in a high-pressure phase, while both $B_{12}S$ and Cu_3N have warnings associated with them in the ICSD indicating a potential problem with the crystal determination for these compounds. We find Cu_3N to be defect tolerant with a band gap around 1.5 eV in agreement with the experimental value for the band gap. Zakutayev *et al.*[43] also categorize the material as defect tolerant and calculate the band gap with G_0W_0 to be around 1 eV.

Some of the candidates reported in Table 1 have been previously explored for different

applications. For example, Cs_3Sb has been investigated experimentally and theoretically as a photocathode.[75–77] We note that De'Munari et al.[78] report a phase transition occurring at around 260 K which could explain the mismatch between the calculated (2.45 eV) and the experimental (1.6 eV at 300K[57]) band gap values for this particular compound. Furthermore, Wu *et al.* explored Cu_2S nanocrystals for PV application[79] whereas Cu_3SbSe_3 and LiBC have been explored as potential thermoelectric and high temperature superconductor, respectively.[62,80–83] Cu_2O has been investigated both in a PV[84] and PEC[85] context. Additionally, attempts have been made to make solar cells out of the ternary compounds of copper, $CuSbSe_2$ and Cu_8Se_6Si.[63,86] Also $CuGaS_2$ have been previously tested for solar hydrogen evolution.[87]

A few of the identified perovskites have been explored actively in recent years. For example, we find $CsSnBr_3$ and $CsSnI_3$ as PV semiconductors having a band gap of $\sim$1.3 eV.[58,88] However, the poor stability of $CsSnX_3$ perovskites in moisture or air prevents them from being used as absorbers in PV devices. Recent suggestions to improve the air stability of the above mentioned perovskites propose Cs_2SnI_6 as a derivative of $CsSnI_3$ which in addition to having improved stability also has high absorption coefficient;[89] we also find Cs_2SnI_6 as one of the possible PV candidates. Two phases of $CsSnI_3$ satisfy the criteria: the orthorhombic so called 'black' phase (1.32 eV band gap) and the tetragonal phase (1.88 eV band gap). However, the most stable $CsSnI_3$ phase, the orthorhombic 'yellow' phase, was not part of the study due to a too high PBE band gap (experimental band gap is 2.6 eV[90]).

In addition to the halogen perovskites, the chalcogen perovskite $BaZrS_3$ has been explored intensively in the last few years as a possible high band gap absorber for water splitting with a band gap of 1.8 eV.[54,91] As Table 1 shows, the screening also identifies $BaZrS_3$ as a potential candidate for PEC application.

The above discussion shows that a few relevant descriptors when used in conjunction lead to a tremendous reduction in the materials space, and that several already known promising materials result from the screening. This provides some credibility to the approach. To shed

Table 2: Calculated properties of known solar energy conversion materials.

Formula	$E_g^{GLLB-SC}$	$E_{g(direct)}^{GLLB-SC}$	m^*_h	m^*_e	$E_g^{exp.}$	defect tolerant
CdSe	1.52	1.52	0.09	0.10	1.73	no
CdTe	1.59	1.59	0.08	0.10	1.43	no
GaAs	0.85	0.85	0.04	0.05	1.42	yes
GaP	2.57	2.81	0.10	0.14	2.3	no
GaInP	1.78	1.78	0.10	0.13	1.81[9]	no
Si	1.11	3.06	0.11	0.56	1.12	no
$CuInSe_2$	1.45	1.45	0.19	0.11	1.01	yes
$BiVO_4$	3.71	3.71	0.46	0.58	2.4-2.5[92]	no

further light on the screening procedure we now briefly discuss a small set of already known PV and PEC materials, which do not appear on the list, and their descriptor values. The materials we consider are Si, GaAs, CdTe, CdSe, GaP, $CuInSe_2$ and $BiVO_4$.

The calculated band gaps and effective masses for these materials are shown in Table 2. They all have energy gaps in either the PV or PEC region in reasonable agreement with experimental values, except for GaP and $BiVO_3$. The band gap of GaP exceeds the 2.5 eV limit by only 0.07 eV, while the discrepancy between the calculated and experimental band gaps for $BiVO_3$ is of the order 1 eV. Wiktor *et al.*[93] have studied the electronic properties of $BiVO_3$ in great detail and find that for this particular material the thermal and zero-point fluctuations lead to a very significant reduction of the calculated band gap by as much as 0.6 - 0.9 eV bringing the calculated gap in considerably better agreement with the experimental value. However, calculation of the thermal effects involve a very time-consuming simulation, which cannot be performed for all compounds in a screening study. All of the effective masses are below the limit of one electron mass used in the screening.

Most of the materials in Table 2 are removed from the screening funnel already at the first step, because As, Bi, Cd, In, and Te are not on the list of accepted chemical elements. GaP is removed because of the band gap slightly above 2.5 eV and would also otherwise have been removed because of defect sensitivity. Last but not least silicon is removed because of defect sensitivity.

In this work we have focussed on identifying light-absorbing materials for PV and PEC

applications taking already synthesized semiconductors of up to three different elements as presented in ICSD as a starting point. Using a set of simple descriptors in a screening funnel the number of compounds is reduced to only 74 candidate materials.

The compounds identified vary a lot in composition, stoichiometry, and structure. They can therefore also be expected to behave very differently with respect to properties not investigated here. This also means that possible synthesis procedures may differ completely from compound to compound and also depend on whether the aim is a bulk material or a thin film of limited thickness. For example, the compounds involving the alkali metals Li, Na, and K or the alkaline earth metals Be, Mg, and Ca may be prone to oxidation and difficult to handle in practice. Also Al may have a problem with instability towards oxidation.

In one of the initial screening steps we removed toxic elements like Cd and As. However, some of the remaining elements can also be toxic in compound form. For example synthesizing phosphides or selenides may – depending on the synthesis procedure – require the handling of phosphine (PH_3) or hydrogen selenide (H_2Se), which are poisonous gases.

Taking these considerations into account we may try to point to some of the materials in Table 1, which can be most easily synthesized and handled. If we for example focus on materials for PEC tandem devices with a band gap of $\sim$ 2 eV and want a material which furthermore will be efficient in thin-film form, the band gap should be direct or at least only slightly indirect. Considering first the binary compounds, which are simpler from a synthesis point of view, we find the materials Hf_3N_4, NbI_5, SrS_3, and Zr_3N_4. None of these have been investigated for PEC before and they all appear promising. Similarly for the ternary compounds we identify the following new (in the context of PEC) compounds: Ba_3SbN, $BaZrN_2$, Cs_6GaSb_3, $CsGeCl_3$, Rb_2SnBr_6, Sr_3GaN_3, and Sr_3SbN. Both Ba_3SbN and Sr_3SbN belong to the class of so-called anti-perovskites, where the cations are on the vertices of the octahedra and the nitrogen in the centers.

It should be noted that even though the number of semiconductors considered here is measured in the thousands, it still only represents a small fraction of the full space of stable

or meta-stable materials. The rather brute-force approach used here, where in principle all materials are investigated, cannot be expected to be applicable to the much larger space of available materials. New approaches based on statistical learning will have to be developed in order to efficiently scan many different crystal structures with different compositions to test for stability.

The descriptors applied in the present work also need to be refined and new descriptors have to be developed for high-throughput screenings. The calculations of the band gaps presented here have rather large uncertainties associated with them, and it is a real challenge to include for example thermal effects as discussed in the case of $BiVO_3$. Furthermore, the band gap itself is only a rough measure of the light absorption properties and even though more sophisticated approaches like time-dependent DFT and the Bethe-Salpeter equations exist, they are still too computationally time-consuming to be applied to many thousand materials.

Defects and interfaces play a major role in optoelectronic device performance, and the present study only addresses the defect issue at the most basic level. Only vacancy defects are studied and only at the level of semi-local functionals. Many other intrinsic defects can be of importance and a more accurate determination of electronic levels in the band gap requires treatments at the non-local DFT or GW level.

Any screening study potentially includes both false-positives and true-negatives and the present study is no exception. There could be many reasons that a material appearing in Table 1, would not work optimally in a real device. However, we think that materials not appearing in the list hardly can be expected to be well-functioning. There might be a few "outliers" where the descriptors fail, but in general the descriptors are conservative. If, for example, the band gap is not in the proper range poor performance can be expected. Similarly if the carrier masses are large, the mobility is expected to be limited and charge extraction will be difficult.

Acknowledgement

Discussions with Gilles Dennler, Andrea Crovetto, and Brian Seger are gratefully acknowledged. The authors acknowledge VILLUM FONDEN for financial support with research grant number 9455. The Center for Nanostructured Graphene is sponsored by the Danish National Research Foundation, Project DNRF103.

The Supporting Information:

Numerical values, ICSD number, and the effective masses of the compounds mentioned in Figure 4 & 5, and Table 1. This material is available free of charge via the Internet at http://pubs.acs.org.

References

(1) Vayssierres, L. *On Solar Hydrogen and Nanotechnology*; John Wiley and Sons (Asia) Pvt. Ltd, 2009.

(2) Chamberlain, G. Organic Solar Cells: A Review. *Sol. Cells* **1983**, *8*, 47–83.

(3) Ni, M.; Leung, M. K.; Leung, D. Y.; Sumathy, K. A Review and Recent Developments in Photocatalytic Water-splitting Using TiO_2 for Hydrogen Production. *Renewable Sustainable Energy Rev.* **2007**, *11*, 401 – 425.

(4) Schmidt-Mende, L.; Fechtenkötter, A.; Müllen, K.; Moons, E.; Friend, R. H.; MacKenzie, J. D. Self-Organized Discotic Liquid Crystals for High-Efficiency Organic Photovoltaics. *Science* **2001**, *293*, 1119–1122.

(5) Kolpak, A. M.; Grossman, J. C. Azobenzene-Functionalized Carbon Nanotubes As High-Energy Density Solar Thermal Fuels. *Nano Lett.* **2011**, *11*, 3156–3162.

(6) Green, M. A. Thin-film Solar Cells: Review of Materials, Technologies and Commercial Status. *J. Mater. Sci.: Mater. Electron.* **2007**, *18*, 15–19.

(7) Green, M. A.; Emery, K.; Hishikawa, Y.; Warta, W.; Dunlop, E. D. Solar Cell Efficiency Tables (Version 45). *Prog. Photovoltaics: Research and Applications* **2015**, *23*, 1–9, PIP-14-274.

(8) Glunz, S. W.; Preu, R.; Biro, D. In *Comprehensive Renewable Energy*; Sayigh, A., Ed.; Elsevier: Oxford, 2012; pp 353–387, DOI: 10.1016/B978-0-08-087872-0.00117-7.

(9) Polman, A.; Knight, M.; Garnett, E. C.; Ehrler, B.; Sinke, W. C. Photovoltaic Materials: Present Efficiencies and Future Challenges. *Science* **2016**, *352*, aad4424.

(10) Kayes, B. M.; Nie, H.; Twist, R.; Spruytte, S. G.; Reinhardt, F.; Kizilyalli, I. C.; Higashi, G. S. *27.6 Percent Conversion Efficiency, A New Record for Single-junction Solar Cells Under 1 Sun Illumination*; 2011 37th IEEE Photovoltaic Specialists Conference, 2011.

(11) Guo, Q.; Ford, G. M.; Yang, W.-C.; Walker, B. C.; Stach, E. A.; Hillhouse, H. W.; Agrawal, R. Fabrication of 7.2% Efficient CZTSSe Solar Cells Using CZTS Nanocrystals. *J. Am. Chem. Soc.* **2010**, *132*, 17384–17386.

(12) Wang, W.; Winkler, M. T.; Gunawan, O.; Gokmen, T.; Todorov, T. K.; Zhu, Y.; Mitzi, D. B. Device Characteristics of CZTSSe Thin-Film Solar Cells with 12.6 % Efficiency. *Adv. Energy Mater.* **2014**, *4*, 1301465.

(13) Walter, M. G.; Warren, E. L.; McKone, J. R.; Boettcher, S. W.; Mi, Q.; Santori, E. A.; Lewis, N. S. Solar Water Splitting Cells. *Chem. Rev.* **2010**, *110*, 6446–6473.

(14) Li, Y.; Zhang, J. Hydrogen Generation from Photoelectrochemical Water Splitting Based on Nanomaterials. *Laser Photonics Rev.* **2010**, *4*, 517–528.

(15) Yokoyama, D.; Minegishi, T.; Jimbo, K.; Hisatomi, T.; Ma, G.; Katayama, M.; Kubota, J.; Katagiri, H.; Domen, K. H_2 Evolution from Water on Modified Cu_2ZnSnS_4 Photoelectrode under Solar Light. *App. Phys. Express* **2010**, *3*, 101202.

(16) Zhang, K.; Ma, M.; Li, P.; Wang, D. H.; Park, J. H. Water Splitting Progress in Tandem Devices: Moving Photolysis beyond Electrolysis. *Adv. Energy Mater.* **2016**, *6*, 1600602.

(17) Brillet, J.; Yum, J.-H.; Cornuz, M.; Hisatomi, T.; Solarska, R.; Augustynski, J.; Graetzel, M.; Sivula, K. Highly Efficient Water Splitting By a Dual-absorber Tandem Cell. *Nat. Photonics* **2012**, *6*, 824–828.

(18) Seger, B.; Castelli, I. E.; Vesborg, P. C. K.; Jacobsen, K. W.; Hansen, O.; Chorkendorff, I. 2-Photon Tandem Device for Water Splitting: Comparing Photocathode First Versus Photoanode First Designs. *Energy Environ. Sci.* **2014**, *7*, 2397–2413.

(19) Pandey, M.; Kuhar, K.; Jacobsen, K. W. II–IV–V2 and III–III–V2 Polytypes as Light Absorbers for Single Junction and Tandem Photovoltaic Devices. *J. Phys. Chem. C* **2017**, *121*, 17780–17786.

(20) Kuhar, K.; Crovetto, A.; Pandey, M.; Thygesen, K. S.; Seger, B.; Vesborg, P. C. K.; Hansen, O.; Chorkendorff, I.; Jacobsen, K. W. Sulfide Perovskites for Solar Energy Conversion Applications: Computational Screening and Synthesis of the Selected Compound $LaYS_3$. *Energy Environ. Sci.* **2017**, *10*, 2579–2593.

(21) Ganose, A. M.; Savory, C. N.; Scanlon, D. O. Beyond Methylammonium Lead Iodide: Prospects for the Emergent Field of ns^2 Containing Solar Absorbers. *Chem. Commun.* **2017**, *53*, 20–44.

(22) Butler, K. T.; Frost, J. M.; Skelton, J. M.; Svane, K. L.; Walsh, A. Computational Materials Design of Crystalline Solids. *Chem. Soc. Rev.* **2016**, *45*, 6138–6146.

(23) Saal, J. E.; Kirklin, S.; Aykol, M.; Meredig, B.; Wolverton, C. Materials Design and Discovery with High-Throughput Density Functional Theory: The Open Quantum Materials Database (OQMD). *JOM* **2013**, *65*, 1501–1509.

(24) Kirklin, S.; Saal, J. E.; Meredig, B.; Thompson, A.; Doak, J. W.; Aykol, M.; Rühl, S.; Wolverton, C. The Open Quantum Materials Database (OQMD): Assessing the Accuracy of DFT Formation Energies. *npj Comput. Mater.* **2015**, *1*, 15010 EP –.

(25) Jain, A.; Ong, S. P.; Hautier, G.; Chen, W.; Richards, W. D.; Dacek, S.; Cholia, S.; Gunter, D.; Skinner, D.; Ceder, G. et al. The Materials Project: A materials genome approach to accelerating materials innovation. *APL Mater.* **2013**, *1*, 011002.

(26) Curtarolo, S.; Setyawan, W.; Hart, G. L.; Jahnatek, M.; Chepulskii, R. V.; Taylor, R. H.; Wang, S.; Xue, J.; Yang, K.; Levy, O. et al. AFLOW: An Automatic Framework for High-throughput Materials Discovery. *Comput. Mater. Sci.* **2012**, *58*, 218–226.

(27) Landis, D. D.; Hummelshøj, J. S.; Nestorov, S.; Greeley, J.; Dulak, M.; Bligaard, T.; Nørskov, J. K.; Jacobsen, K. W. The Computational Materials Repository. *Comput. Sci. Eng.* **2012**, *14*, 51.

(28) Ghiringhelli, L. M.; Carbogno, C.; Levchenko, S.; Mohamed, F.; Huhs, G.; Lüders, M.; Oliveira, M.; Scheffler, M. Towards Efficient Data Exchange and Sharing for Big-data Driven Materials Science: Metadata and Data Formats. *npj Comput. Mater.* **2017**, *3*, 46.

(29) Kresse, G.; Joubert, D. From Ultrasoft Pseudopotentials to the Projector Augmented-wave Method. *Phys. Rev. B* **1999**, *59*, 1758–1775.

(30) Mortensen, J. J.; Hansen, L. B.; Jacobsen, K. W. Real-space Grid Implementation of the Projector Augmented Wave Method. *Phys. Rev. B* **2005**, *71*, 35109.

(31) Enkovaara, J.; Rostgaard, C.; Mortensen, J. J.; Chen, J.; Dułak, M.; Ferrighi, L.; Gavnholt, J.; Glinsvad, C.; Haikola, V.; Hansen, H. A. et al. Electronic Structure Calculations with GPAW: A Real-space Implementation of the Projector Augmented-wave Method. *J. Phys.: Condens. Matter* **2010**, *22*, 3202.

(32) Bahn, S. R.; Jacobsen, K. W. An Object-Oriented Scripting Interface to a Legacy Electronic Structure Code. *Comput. Sci. Eng.* **2002**, *4*, 56–66.

(33) Larsen, A.; Mortensen, J.; Blomqvist, J.; Castelli, I. E.; Christensen, R.; Dulak, M.; Friis, J.; Groves, M.; Hammer, B.; Hargus, C. et al. The atomic simulation environment—a Python library for working with atoms. *J. Phys.: Condens. Matter* **2017**, *29*, 273002.

(34) Monkhorst, H. J.; Pack, J. D. Special Points for Brillouin-zone Integrations. *Phys. Rev. B* **1976**, *13*, 12.

(35) Gritsenko, O.; van Leeuwen, R.; van Lenthe, E.; Baerends, E. J. Self-consistent Approximation to the Kohn-Sham Exchange Potential. *Phys. Rev. A* **1995**, *51*, 1944.

(36) Kuisma, M.; Ojanen, J.; Enkovaara, J.; Rantala, T. T. Kohn-Sham Potential with Discontinuity for Band Gap Materials. *Phys. Rev. B* **2010**, *82*, 115106.

(37) Castelli, I. E.; Hüser, F.; Pandey, M.; Li, H.; Thygesen, K. S.; Seger, B.; Jain, A.; Persson, K. A.; Ceder, G.; Jacobsen, K. W. New Light-Harvesting Materials Using Accurate and Efficient Bandgap Calculations. *Adv. Energy Mater.* **2015**, *5*, 1400915.

(38) Perdew, J. P.; Burke, K.; Ernzerhof, M. Generalized Gradient Approximation Made Simple. *Phys. Rev. Lett.* **1996**, *77*, 3865–3868.

(39) Bergerhoff, G.; Hundt, R.; Sievers, R.; Brown, I. D. The Inorganic Crystal Structure Data Base. *J. Chem. Inf. Comput. Sci.* **1983**, *23*, 66–69.

(40) Gaultois, M. W.; Sparks, T. D.; Borg, C. K. H.; Seshadri, R.; Bonificio, W. D.; Clarke, D. R. Data-Driven Review of Thermoelectric Materials: Performance and Resource Considerations. *Chem. Mater.* **2013**, *25*, 2911–2920.

(41) Setyawan, W.; Curtarolo, S. High-throughput Electronic Band Structure Calculations: Challenges and Tools. *Comput. Mater. Sci.* **2010**, *49*, 299–312.

(42) Shukla, S.; Xing, G.; Ge, H.; Prabhakar, R. R.; Mathew, S.; Su, Z.; Nalla, V.; Venkatesan, T.; Mathews, N.; Sritharan, T. et al. Origin of Photocarrier Losses in Iron Pyrite (FeS_2) Nanocubes. *ACS Nano* **2016**, *10*, 4431–4440.

(43) Zakutayev, A.; Caskey, C. M.; Fioretti, A. N.; Ginley, D. S.; Vidal, J.; Stevanovic, V.; Tea, E.; Lany, S. Defect Tolerant Semiconductors for Solar Energy Conversion. *J. Phys. Chem. Lett.* **2014**, *5*, 1117–1125.

(44) Pandey, M.; Rasmussen, F. A.; Kuhar, K.; Olsen, T.; Jacobsen, K. W.; Thygesen, K. S. Defect-Tolerant Monolayer Transition Metal Dichalcogenides. *Nano Lett.* **2016**, *16*, 2234–2239.

(45) Walsh, A.; Zunger, A. Instilling Defect Tolerance in New Compounds. *Nat. Mater.* **2017**, *16*, 964–967.

(46) Pandey, M.; Jacobsen, K. W.; Thygesen, K. S. Band Gap Tuning and Defect Tolerance of Atomically Thin Two-Dimensional Organic–Inorganic Halide Perovskites. *J. Phys. Chem. Lett.* **2016**, *7*, 4346–4352.

(47) Lany, S.; Zunger, A. Assessment of Correction Methods for the Band-gap Problem and for Finite-size Effects in Supercell Defect Calculations: Case Studies for ZnO and GaAs. *Phys. Rev. B* **2008**, *78*, 235104.

(48) Freysoldt, C.; Neugebauer, J.; Van de Walle, C. G. Fully *Ab Initio* Finite-Size Corrections for Charged-Defect Supercell Calculations. *Phys. Rev. Lett.* **2009**, *102*, 016402.

(49) Komsa, H.-P.; Rantala, T. T.; Pasquarello, A. Finite-size Supercell Correction Schemes for Charged Defect Calculations. *Phys. Rev. B* **2012**, *86*, 045112.

(50) Schultz, P. A. Charged Local Defects in Extended Systems. *Phys. Rev. Lett.* **2000**, *84*, 1942–1945.

(51) Goyal, A.; Gorai, P.; Peng, H.; Lany, S.; Stevanović, V. A Computational Framework for Automation of Point Defect Calculations. *Comput. Mater. Sci.* **2017**, *130*, 1–9.

(52) Larsen, A. H.; Vanin, M.; Mortensen, J. J.; Thygesen, K. S.; Jacobsen, K. W. Localized Atomic Sasis Set in the Projector Augmented Wave Method. *Phys. Rev. B* **2009**, *80*, 195112.

(53) Ropp, R. C. *Encyclopedia of the Alkaline Earth Compounds*; Newnes, 2012; Google-Books-ID: yZ786vEild0C.

(54) Niu, S.; Huyan, H.; Liu, Y.; Yeung, M.; Ye, K.; Blankemeier, L.; Orvis, T.; Sarkar, D.; Singh, D. J.; Kapadia, R. et al. Bandgap Control via Structural and Chemical Tuning of Transition Metal Perovskite Chalcogenides. *Adv. Mater.* **2017**, *29*, 1604733.

(55) 2.08 eV obtained with HSE06 functional.

(56) Wang, A.; Yan, X.; Zhang, M.; Sun, S.; Yang, M.; Shen, W.; Pan, X.; Wang, P.; Deng, Z. Controlled Synthesis of Lead-Free and Stable Perovskite Derivative Cs_2SnI_6 Nanocrystals via a Facile Hot-Injection Process. *Chem. Mater.* **2016**, *28*, 8132–8140.

(57) Madelung, O. *Semiconductors Data Handbook*; Springer: Berlin, 2004; pp 815–835.

(58) Moghe, D.; Wang, L.; Traverse, C. J.; Redoute, A.; Sponseller, M.; Brown, P. R.; Bulović, V.; Lunt, R. R. All Vapor-deposited Lead-free Doped $CsSnBr_3$ Planar Solar Cells. *Nano Energy* **2016**, *28*, 469–474.

(59) Huang, L.-y.; Lambrecht, W. R. L. Electronic Band Structure, Phonons, and Exciton Binding Energies of Halide Perovskites $CsSnCl_3$, $CsSnBr_3$, and $CsSnI_3$. *Phys. Rev. B* **2013**, *88*, 165203.

(60) Yu, C.; Chen, Z.; Wang, J. J.; Pfenninger, W.; Vockic, N.; Kenney, J. T.; Shum, K. Temperature Dependence of the Band Gap of Perovskite Semiconductor Compound $CsSnI_3$. *J. App. Phys.* **2011**, *110*, 063526–063526.

(61) Kim, K. J.; Kim, J. H.; Kang, J. H. Structural and Optical Characterization of Cu_3N Films Prepared by Reactive RF Magnetron Sputtering. *J. Cryst. Growth* **2001**, *222*, 767 – 772.

(62) Fernández, A. M.; Turner, J. A. Preparation and Photocharacterization of Cu–Sb–Se Films by Electrodeposition Technique. *Sol. Energy Mater. Sol. Cells* **2003**, *79*, 391–399.

(63) Brammertz, G.; Vermang, B.; ElAnzeery, H.; Sahayaraj, S.; Ranjbar, S.; Meuris, M.; Poortmans, J. Fabrication and Characterization of Ternary Cu_8SiS_6 and Cu_8SiSe_6 Thin Film Layers for Optoelectronic Applications. *Thin Solid Films* **2016**, *616*, 649–654.

(64) Tell, B.; Shay, J. L.; Kasper, H. M. Electrical Properties, Optical Properties, and Band Structure of $CuGaS_2$ and $CuInS_2$. *Phys. Rev. B* **1971**, *4*, 2463–2471.

(65) Colombara, D.; Peter, L. M.; Rogers, K. D.; Painter, J. D.; Roncallo, S. Formation of $CuSbS_2$ and $CuSbSe_2$ Thin Films via Chalcogenisation of Sb–Cu Metal Precursors. *Thin Solid Films* **2011**, *519*, 7438–7443.

(66) Yablonskikh, M.; Dzivenko, D.; Bourguille, J.; Riedel, R.; Magnano, E.; Parmigiani, F.; Zerr, A. Electronic Structure and Band Gap of Oxygen Bearing c-Zr_3N_4 and of c-Hf_3N_4 by Soft X-ray Spectroscopy. *Phys. Status Solidi A* **2014**, *211*, 835–842.

(67) Kuriyama, K.; Kato, T.; Tanaka, T. Optical Band gap of the Filled Tetrahedral Semiconductor LiZnN. *Phys. Rev. B* **1994**, *49*, 4511–4513.

(68) Kuriyama, K.; Taguchi, R.; Kushida, K.; Ushiyama, K. Growth and Band gap of the Filled Tetrahedral Semiconductor LiZnN. *J. Cryst. Growth* **1999**, *198*, 802–805.

(69) Watson, L. M.; Marshall, C. A. W.; Cardoso, C. P. On the Electronic Structure of the Semiconducting Compounds Mg_3Bi_2 and Mg_3Sb_2. *J. Phys. F: Met. Phys.* **1984**, *14*, 113.

(70) Gäbler, F.; Kirchner, M.; Schnelle, W.; Schwarz, U.; Schmitt, M.; Rosner, H.; Niewa, R. Sr_3NE and Ba_3NE (E = Sb, Bi): Synthesis, Crystal Structures, and Physical Properties. *Z. Anorg. Allg. Chem.* **2004**, *630*, 2292–2298.

(71) Olsson, P.; Vidal, J.; Lincot, D. Ab initio Study of II–VI_2 Dichalcogenides. *J. Phys.: Condens. Matter* **2011**, *23*, 405801.

(72) Johansson, B.; Hentzell, H.; Harper, J.; Cuomo, J. Higher Nitrides of Hafnium, Zirconium, and Titanium Synthesized by Dual Ion Beam Deposition. *J. Mater. Res.* **1986**, *1*, 442–451.

(73) Guthrie, D. H.; Corbett, J. D. Synthesis and Structure of An Infinite-chain Form of ZrI_2 (α). *J. Solid State Chem.* **1981**, *37*, 256 – 263.

(74) Moustafa, M.; Zandt, T.; Janowitz, C.; Manzke, R. Growth and Band Gap Determination of the ZrS_xSe_{2-x} Single Crystal Series. *Phys. Rev. B* **2009**, *80*, 035206.

(75) Kalarasse, L.; Bennecer, B.; Kalarasse, F. Optical Properties of the Akali Antimonide Semiconductors Cs_3Sb, Cs_2KSb, CsK_2Sb and K_3Sb. *J. Phys. Chem. Solids* **2010**, *71*, 314–322.

(76) Spicer, W. E. Photoemissive, Photoconductive, and Optical Absorption Studies of Alkali-Antimony Compounds. *Phys. Rev.* **1958**, *112*, 114–122.

(77) Wei, S.-H.; Zunger, A. Electronic Structure of M_3ISb-type Filled Tetrahedral Semiconductors. *Phys. Rev. B* **1987**, *35*, 3952–3961.

(78) De'Munari, G. M.; Mambriani, G.; Giusiano, F. Photoemissive Yield of Cs_3Sb Photocathode and Its Dependence on Temperature. *Rev. Sci. Instrum.* **1967**, *38*, 1128–1132.

(79) Wu, Y.; Wadia, C.; Ma, W.; Sadtler, B.; Alivisatos, A. P. Synthesis and Photovoltaic Application of Copper(I) Sulfide Nanocrystals. *Nano Lett.* **2008**, *8*, 2551–2555.

(80) Lazicki, A.; Yoo, C.-S.; Cynn, H.; Evans, W. J.; Pickett, W. E.; Olamit, J.; Liu, K.; Ohishi, Y. Search for Superconductivity in LiBC at High Pressure: Diamond Anvil Cell Experiments and First-principles Calculations. *Phys. Rev. B* **2007**, *75*, 054507.

(81) Rosner, H.; Kitaigorodsky, A.; Pickett, W. E. Prediction of High T_c Superconductivity in Hole-Doped LiBC. *Phys. Rev. Lett.* **2002**, *88*, 127001.

(82) Caputo, R. Exploring the Structure-composition Phase Space of Lithium Borocarbide, Li_xBC for $x \leq 1$. *RSC Adv.* **2013**, *3*, 10230–10241.

(83) Miao, R.; Yang, J.; Jiang, M.; Zhang, Q.; Cai, D.; Fan, C.; Bai, Z.; Liu, C.; Wu, F.; Ma, S. First-principles Study of Superconductivity in the Hole Self-doped $LiB_1.1C_0.9$. *J. App. Phys.* **2013**, *113*, 133910.

(84) Briskman, R. N. A Study of Electrodeposited Cuprous-Oxide Photovoltaic Cells. *Sol. Energy Mater. Sol. Cells* **1992**, *27*, 361–368.

(85) Liu, Y.; Yang, G.; Zhang, H.; Cheng, Y.; Chen, K.; Peng, Z.; Chen, W. Enhanced Visible Photocatalytic Activity of Cu_2O Nanocrystal/Titanate Nanobelt Heterojunctions by a Self-assembly Process. *RSC Adv.* **2014**, *4*, 24363–24368.

(86) Welch, A. W.; Baranowski, L. L.; Zawadzki, P.; Lany, S.; Wolden, C. A.; Zakutayev, A. $CuSbSe_2$ Photovoltaic Devices with 3% Efficiency. *Appl. Phys. Express* **2015**, *8*, 082301.

(87) Iwase, A.; Ng, Y. H.; Amal, R.; Kudo, A. Solar Hydrogen Evolution Using a $CuGaS_2$ Photocathode Improved by Incorporating Reduced Graphene Oxide. *J. Mater. Chem. A* **2015**, *3*, 8566–8570.

(88) Song, T.-B.; Yokoyama, T.; Aramaki, S.; Kanatzidis, M. G. Performance Enhancement of Lead-Free Tin-Based Perovskite Solar Cells with Reducing Atmosphere-Assisted Dispersible Additive. *ACS Energy Lett.* **2017**, *2*, 897–903.

(89) Qiu, X.; Cao, B.; Yuan, S.; Chen, X.; Qiu, Z.; Jiang, Y.; Ye, Q.; Wang, H.; Zeng, H.; Liu, J. et al. From Unstable $CsSnI_3$ to Air-stable Cs_2SnI_6: A Lead-free Perovskite Solar Cell Light Absorber with Bandgap of 1.48 eV and High Absorption Coefficient. *Sol. Energy Mater. Sol. Cells* **2017**, *159*, 227–234.

(90) da Silva, E. L.; Skelton, J. M.; Parker, S. C.; Walsh, A. Phase Stability and Transformations in the Halide Perovskite $CsSnI_3$. *Phys. Rev. B* **2015**, *91*, 144107.

(91) Meng, W.; Saparov, B.; Hong, F.; Wang, J.; Mitzi, D. B.; Yan, Y. Alloying and Defect Control within Chalcogenide Perovskites for Optimized Photovoltaic Application. *Chem. Mater.* **2016**, *28*, 821–829.

(92) Cooper, J. K.; Gul, S.; Toma, F. M.; Chen, L.; Glans, P.-A.; Guo, J.; Ager, J. W.; Yano, J.; Sharp, I. D. Electronic Structure of Monoclinic $BiVO_4$. *Chem. Mater.* **2014**, *26*, 5365–5373.

(93) Wiktor, J.; Reshetnyak, I.; Ambrosio, F.; Pasquarello, A. Comprehensive Modeling of the Band Gap and Absorption Spectrum of $BiVO_4$. *Phys. Rev. Mater.* **2017**, *1*, 022401.